Dynamics of dark hollow Gaussian laser pulses in relativistic plasma

A. Sharma,[1,*] S. Misra,[2] S. K. Mishra,[3] and I. Kourakis[4]
[1]*Institute of Physics, University of Pecs, 7621 Pecs, Hungary*
[2]*Centre for Energy Studies, IIT Delhi, Hauz Khas, New Delhi, India*
[3]*Institute for Plasma Research, Gandhinagar, India*
[4]*Centre for Plasma Physics, School of Mathematics and Physics, Queen's University Belfast, BT7 1NN Belfast, Northern Ireland, United Kingdom*

(Received 15 February 2013; revised manuscript received 22 April 2013; published 25 June 2013)

Optical beams with null central intensity have potential applications in the field of atom optics. The spatial and temporal evolution of a central shadow dark hollow Gaussian (DHG) relativistic laser pulse propagating in a plasma is studied in this article for first principles. A nonlinear Schrodinger-type equation is obtained for the beam spot profile and then solved numerically to investigate the pulse propagation characteristics. As series of numerical simulations are employed to trace the profile of the focused and compressed DHG laser pulse as it propagates through the plasma. The theoretical and simulation results predict that higher-order DHG pulses show smaller divergence as they propagate and, thus, lead to enhanced energy transport.

DOI: 10.1103/PhysRevE.87.063111 PACS number(s): 52.38.−r, 52.35.−g, 52.90.+z, 03.75.Be

I. INTRODUCTION

There are various techniques for trapping individual atoms or atom clouds in isolation. In a recent investigation, Goban *et al.* [1] introduced an improved technique for trapping a cesium atom approximately 200 nm from the surface of a dielectric nanofiber in a way that is less disruptive to the atom than earlier approaches. A method of stabilized trapping, cooling, and manipulating atoms on a continuous-wave basis was proposed at an early stage in Ref. [2], relying on resonance radiation pressure forces. That study predicted the use of highly focused laser beams and atomic beam injection on a very deep trap for confining single atoms or gases at temperatures 10^{-6} K. Numerous important advances have been made by loading ultracold atoms inside hollow-core optical fibers [3–5] and by trapping atoms in the evanescent fields of nanoscale waveguides [6,7].

In recent years, optical beams with zero central intensity [8] have attracted much attention because of their increasing application in atom optics. Theoretical and experimental studies show that the dipole potentials in the hollow beams can be used to guide and trap atoms [9–13]. It has been reported that an ultracold atomic sample was obtained in a pyramidal hollow beam dipole trap and that an all-optical-type Bose Einstein condensate was achieved in a far-blue-detuned hollow beam trap [14].

Another promising technique [15] for optical applications relies on optically tunable hollow Gaussian beams created by phase distortion when a Gaussian beam is reflected off metal films. To describe a dark hollow beam (a beam with zero central intensity), various theoretical models have been introduced, such as the TEM_{01}-mode doughnut beam [16], higher-order Bessel beams [17], and superpositions of off-axis Gaussian beams [12–19] and of dark-hollow Gaussian beams [8,20,21]; in particular the dark hollow Gaussian beams (HGBs) can be expressed as a superposition of a series of Laguerre Gaussian modes [8]. Numerous methods and experimental techniques such as the geometrical optical method [10], optical holography [22], transverse mode selection [23,24], fiber waveguide [25], computer-generated hologram (CGH) [26,27], and spatial filtering [28] have been utilized to generate DHGB. In most experimental realizations of hollow beams the intensity at the center is not absolutely zero, nor can the beam retain a minimum intensity at its center as it propagates in free space or medium. In order to provide a physical description of DHB propagation dynamics and for the sake of simplicity in the analysis, the mathematical model introduced by Cai *et al.* [8] is used in our study to describe a central dark hollow Gaussian beam (DHGB). Such Gaussian symmetric off-axis intensity profile beams can experimentally be generated by using the microcollimation technique for the output beam of micron-sized hollow-optical-fiber waveguides [25]. The propagation of dark hollow beams in paraxial optical systems (including turbulent atmosphere) has been investigated in various studies in the past [21,29–33].

In a recent investigation [34] the focusing of HGBs in plasma was studied, considering collisional, ponderomotive, and relativistic nonlinearities. The work also reported the effect of the order of HGBs and of the nature of nonlinearity on self-focusing of the beam. Another work by the same group [35] investigated the self-focusing of a HGB in a magnetoplasma, considering ponderomotive and collisional nonlinearities. Misra and Mishra [36] further analyzed the paraxial like approach to study the propagation of various order HGBs, in a homogeneous plasma, where both relativistic and ponderomotive nonlinearities are simultaneously present. The study of focusing dark hollow beams is also important in atmospheric propagation. In a recent work [37] the focusing of a HGB laser in atmospheric environments is investigated. It was argued that dark hollow beams are less divergent in comparison to Gaussian shaped beams. Consequently, HGB laser beams may be employed for enhanced energy transport at remote distances in atmosphere.

A review of the literature reveals the fact that the propagation characteristics of dark hollow Gaussian (DHG) pulse in a plasma or other nonlinear media have not been studied to a

*Corresponding author: a_physics2001@yahoo.com

significant extent; as an exception, the propagation properties of the hollow Gaussian pulsed beams in free space were studied in Ref. [38].

In this article, we focus our attention for the spatiotemporal evolution of the DHG pulse in plasma medium at relativistic intensity. Relativistic mass variation during laser-plasma interaction is the origin of longitudinal self-compression of a laser pulse down to a single laser cycle in length, with a corresponding increase in intensity. The main source of nonlinearity is the relativistic mass increase due to the quiver motion of the electrons in the field of the laser. In the past few years, several situations have been proposed for the spatiotemporal evolution of a Gaussian laser pulse in plasma [39]. Shorokhov *et al.* [40] have employed a 3D particle-in-cell simulation to show that a 30-fs-long laser pulse is efficiently compressed to 5 fs by using a periodic plasma-vacuum structure to damp filamentation. Tsung *et al.* [41] reported a scheme to generate single-cycle laser pulses based on photon deceleration in underdense plasmas. This robust and tunable process is ideally suited for lasers above critical power because it takes advantage of the relativistic self-focusing of these lasers and the nonlinear features of the plasma wake. Ren *et al.* [42] demonstrated the compression and focusing of a short laser pulse by a thin plasma lens. A set of analytical expressions for the spot size and for the length evolution of a short laser pulse were derived in their model. Shibu *et al.* [43] also proposed the possibility of pulse compression in relativistic homogeneous plasma and investigated the interplay between transverse focusing and longitudinal compression.

The vast majority of earlier works outlined above have considered the pulse self-compression of a Gaussian laser beam in a homogeneous relativistic plasma. We focus here on the spatiotemporal dynamics of DHG pulses, an aspect not covered earlier to our knowledge. We rely on a nonlinear Schrodinger equation (NLSE) formal description to study the spatiotemporal dynamics of the *em* field envelope. Following Refs. [44–46], we introduce a set of trial functions via the intensity profile of the laser pulse and follow their evolution in space and time in the plasma. We adopt a three-dimensional (3D) model, relying on the *em* wave equation as derived from Maxwell's equations. A nonlinear Schrodinger equation is then obtained and solved by using the paraxial formalism to model the occurrence of longitudinal pulse width compression and associated energy localization. A pair of appropriate trial functions are defined, accounting for the beam width (in space) and the pulse duration (in time), whose evolution describes the dynamics of the DHG pulse. Both longitudinal and transverse self-compression are examined for a finite extent dark hollow Gaussian laser pulse through this model. These functions are determined by a system of coupled nonlinear differential equations, which are integrated numerically to yield the spatiotemporal behavior of the DHG laser pulse profile.

We have investigated here the spatiotemporal dynamics of a weakly relativistic DHG laser pulse in a narrow window of plasma density values from 0.25 n_c to slightly below n_c, where $n_c = m_e\omega^2/4\pi e^2$ is the critical plasma density for a laser pulse with frequency $\omega = 2\pi c/\lambda$. In this density region, the Raman instability [47] that otherwise destroys the pulse is impeded. In particular, the Raman instability, most simply characterized as the resonant decay of an incident photon into a scattered photon and an electron plasma wave (or plasmon), relies on the frequency and wave number matching conditions, viz., $\omega_0 = \omega_s + \omega_{pe}$ and $k_0 = k_s + k$, where the subscripts "0" and "s" denote the incident and the scattered light wave, respectively. Since the minimum frequency of a light wave in a plasma is $\omega_{\rm pe}$ (the electron plasma frequency), it is clear that Raman instability requires strongly underdense conditions, such that $n \ll n_{\rm cr}/4$, where n is the plasma density and $n_{\rm cr}$ is the critical density.

In the article at hand, we have adopted a simplified analytical formalism by considering only weak relativistic nonlinearity effects to a first approach. Accordingly, we have neglected electron density perturbations, thus ruling out Raman hosing and other instabilities [47–49]. This assumption is valid for long laser pulses [$c \times$ (pulse duration) $\gg$ (plasma wavelength)] and for plasma densities above $n_c/4$, where Raman instabilities are prohibited. Given the physical constraints discussed above, we have investigated DHG pulse dynamics while assuming a weakly relativistic normalized laser field ($a < 1$), with a pulse length that is much larger than the plasma wavelength and a plasma density ranging from quarter-critical to the critical value. The normalized laser field amplitude (a) discussed above can be expressed, for the sake of clarity, as $a = eA_{00}/m\omega c = 8.5 \times 10^{-10}\sqrt{I(\mathrm{Wcm}^{-2})}\lambda(\mu\mathrm{m})$, where A_{00} is the laser field amplitude at $z = 0$ [refer to Eq. (24) below]. The analytical model successfully shows the spatiotemporal focusing dynamics of DHG pulse in weakly relativisitc regime $a < 1$. Assuming a weakly relativistic field, one may neglect the momentum acquired by the electrons along the laser propagation direction due to the $\mathbf{v} \times \mathbf{B}$ term, otherwise accumulation of electrons ahead of pulse may destroy it at strong laser fields. The weak-field regime also favors the applicability of the paraxial approach throughout propagation. Our numerical results (shown in Sec. III) also confirm the applicability of the model for weakly relativistic fields.

II. ANALYTICAL MODEL

We consider the propagation of a circularly polarized dark hollow Gaussian pulse along the z direction. The electric field vector for the electromagnetic pulse can be written as

$$E(r, z, t) = A(r, z, t)\,(e_x + ie_y)\,\exp\left[i(kz - \omega t)\right], \quad (1)$$

where

$$A(r, z = 0, t) = A_{00}\left(-\frac{r^2}{2r_0^2}\right)^n \exp\left(-\frac{r^2}{2r_0^2}\right)\exp\left(-\frac{t^2}{2\tau_0^2}\right), \quad (2)$$

In the above expressions A refers to the complex amplitude of the hollow Gaussian pulse of initial beam width r_0 (in space) and initial pulse width τ_0 (in time); A_{00} is a real constant characterizing the amplitude of the DHG pulse; n is a positive integer, characterizing the shape of the DHG pulse and the position of its maximum; and ω and k are, respectively, the frequency and wave number of pulse. The wave number of the electromagnetic beam satisfies the plasma dispersion relation, $c^2k^2 = \omega^2 - \omega_p^2$, where ω_p is the plasma frequency. We show in Fig. 1 the normalized laser field amplitude $[A(z = 0)/A_{00}]$

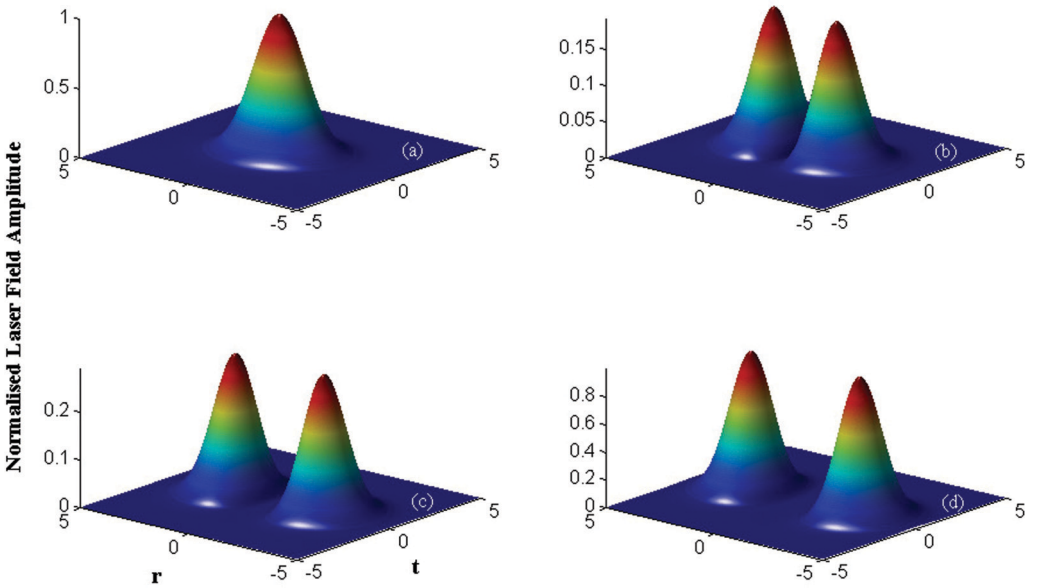

FIG. 1. (Color online) The normalized laser field amplitude of a dark hollow Gaussian laser pulse is depicted for (a) $n = 0$ (Gaussian), (b) 1, (c) 2, and (d) 3.

plots for a DHG pulse of order $n = 0$ (Gaussian), 1, 2, and 3. It can be observed from the DHG pulse profile that a dark region increases with a higher order of a DHG pulse. We note that one readily recovers the known expression for a fundamental Gaussian pulse for setting $n = 0$ in Eq. (2) above.

The electric field vector E satisfies the wave equation [45],

$$2\,i\,k\,\frac{\partial A}{\partial z} + \frac{\partial^2 A}{\partial \tau^2} + \left(\frac{\partial^2 A}{\partial^2 r} + \frac{1}{r}\frac{\partial A}{\partial r}\right) + \phi(|A|^2)A = 0, \tag{3}$$

where we have introduced the new dimensionless variable as $\tau = (t - z/v_g)c$.

Equation (3) is formally a nonlinear Schrodinger equation including terms taking into account both longitudinal compression and transverse self-focusing. The second term in Eq. (3) is known as the group velocity dispersion (GVD) term and it results in pulse compression when combined with (balanced by) nonlinearity. The third term in the above equation (within parentheses) physically represents diffraction, which is necessary for transverse focusing. The last term in Eq. (3) represents the nonlinear effect, which arises from the relativistic motion of the electrons in the intense laser field and expressed as [46]

$$\varepsilon = \varepsilon_0 + \phi(|A|^2), \tag{4}$$

where

$$\varepsilon_0 = 1 - \left(\omega_p^2/\omega^2\right), \tag{5}$$

$$\phi(|A|^2) = \frac{\omega_p^2}{\omega^2}\frac{\gamma - 1}{\gamma}, \tag{6}$$

and

$$\gamma = \left(1 + \frac{e^2(|A|^2)}{m^2\omega^2c^2}\right)^{1/2}. \tag{7}$$

The solution of Eq. (3) can be expressed as

$$A(r,z,\tau) = A_0(r,z,\tau)\,\exp[-ikS(r,z,\tau)], \tag{8}$$

where both amplitude (A_0) and eikonal (S) are real quantities. The eikonal S is related with the curvature of the wavefront, while the amplitude (square) represents the intensity profile. Substituting for A from Eq. (8) in Eq. (3) and separating the real from the imaginary parts, one obtains

$$\frac{\partial A_0^2}{\partial z} + \frac{\partial S}{\partial r}\frac{\partial A_0^2}{\partial r} + A_0^2\left(\frac{\partial^2 S}{\partial r^2} + \frac{1}{r}\frac{\partial S}{\partial r}\right) + \frac{\partial S}{\partial \tau}\frac{\partial (A_0^2)}{\partial \tau} + A_0^2\left(\frac{\partial^2 S}{\partial \tau^2}\right) = 0 \tag{9}$$

and

$$2\frac{\partial S}{\partial z} + \left(\frac{\partial S}{\partial r}\right)^2 + \left(\frac{\partial S}{\partial \tau}\right)^2 = \frac{\omega^2\phi(|A|^2)A_0}{c^2k^2} + \frac{1}{k^2A_0}\left[\left(\frac{\partial^2 A_0}{\partial r^2} + \frac{1}{r}\frac{\partial A_0}{\partial r}\right) + \left(\frac{\partial^2 A_0}{\partial \tau^2}\right)\right]. \tag{10}$$

Adopting an approach analogous to paraxial theory [34,35,45], we anticipate a solution for Eqs. (9) and (10). Thus, one may start by expressing Eqs. (9) and (10) in terms of the radial variables η and propagation distance z, where

$$\eta = \frac{r}{r_0 f(z)} - \sqrt{2n}, \tag{11}$$

In the above expression η is a reduced radial coordinate and $f(z)$ is the beam width parameter [defined by Eqs. (14) and (25)]. $r_0 f(z)$ is the width of the beam and $r = r_0 f\sqrt{2n}$ is the position of the maximum irradiance for the propagating beam; it is shown later that in the paraxial-like approximation, i.e., when $\eta \ll \sqrt{2n}$, Eqs. (9) and (10) lead to the maintenance of the DHG pulse character during propagation. Since the irradiance of the beam is a function of r and z only, expansions of expressions for relevant parameters made along r, near the irradiance maximum viz. $r = r_0 f(z)\sqrt{2n}$, are

certainly justified in the paraxial-like approximation; for $n = 0$ (Gaussian beam), the expansion is made (likewise) around $r = 0$ (as usual). In the framework of the paraxial theory, the present analysis is strictly applicable when $\eta \ll \sqrt{2n}$. Thus, using the expansion (11) in terms of η we may express Eqs. (9) and (10) as

$$\frac{\partial A_0^2}{\partial z} + \frac{1}{r_0^2 f^2}\frac{\partial S}{\partial \eta}\frac{\partial A_0^2}{\partial \eta} + \frac{A_0^2}{r_0^2 f^2}\left[\frac{\partial^2 S}{\partial \eta^2} + \frac{1}{(\sqrt{2n}+\eta)}\frac{\partial S}{\partial \eta}\right] + \frac{\partial S}{\partial \tau}\frac{\partial (A_0^2)}{\partial \tau} + A_0^2\left(\frac{\partial^2 S}{\partial \tau^2}\right) = 0 \tag{12}$$

and

$$2\frac{\partial S}{\partial z} + \frac{1}{r_0^2 f^2}\left(\frac{\partial S}{\partial \eta}\right)^2 + \left(\frac{\partial S}{\partial \tau}\right)^2 = \frac{\omega^2 \phi(|A|^2)A_0}{c^2 k^2} + \frac{1}{k^2 A_0 r_0^2 f^2}\left[\frac{\partial^2 A_0}{\partial \eta^2} + \frac{1}{(\sqrt{2n}+\eta)}\frac{\partial A_0}{\partial \eta}\right] + \frac{1}{k^2 A_0}\left(\frac{\partial^2 A_0}{\partial \tau^2}\right). \tag{13}$$

Following the paraxial approach [45,46], one may anticipate the solution of Eq. (12) in the following form:

$$A_0^2(r,z,\tau) = \frac{A_{00}^2}{2^{2n} g(z) f(z)^2}(\sqrt{2n}+\eta)^{4n} \exp\left[-(\sqrt{2n}+\eta)^2\right] \times \exp\left[\frac{-\tau^2}{\tau_L^2 g(z)^2}\right] \tag{14}$$

and

$$S(r,z,\tau) = \frac{(\sqrt{2n}+\eta)^2 r_0^2 f}{2}\frac{df}{dz} + \frac{\tau^2}{2g}\frac{dg}{dz} + \varphi(z), \tag{15}$$

where $f(z)$ and $g(z)$ are beam width (space) and pulse width (time) parameters, whose evolution [governed by Eqs. (25) and (26), see below] determines the pulse dynamics. $\tau_L = c\tau_0$ is the pulse length. Identifying the components of the eikonal (S) in the latter expression, the first two terms above are indicative of the spherical curvature of the wavefront, while φ represents its departure from the spherical nature.

In the paraxial-like approximation the relevant parameters [i.e., the dielectric function $\varepsilon(\eta,z,\tau)$, eikonal and irradiance] may be expanded around the maximum of the DHG pulse, i.e., around $\eta = 0$ and $\tau = 0$, where $\eta = r/r_0 f(z) - \sqrt{2n}$. Thus, one can express the effective dielectric function $\varepsilon(\eta,z,\tau)$ around the maximum $\eta = 0, \tau = 0$ of the DHG pulse as

$$\varepsilon = \varepsilon_0(z) - \eta^2 \varepsilon_{2\eta}(z) - \tau^2 \varepsilon_{2\tau}(z). \tag{16}$$

Using Eqs. (8), (14), (15), and (16), the spatiotemporal evolution of the DHG pulse in the plasma can be written as

$$EE^* = A^2(\eta,z,\tau) = \frac{A_{00}^2}{2^{2n} g(z) f(z)^2}(\sqrt{2n}+\eta)^{4n} \times \exp\left[-(\sqrt{2n}+\eta)^2\right]\exp\left[\frac{-\tau^2}{\tau_L^2 g(z)^2}\right]. \tag{17}$$

To obtain the coefficient of effective dielectric function (16) one may expand EE^* in powers of η^2 and τ^2 following (17),

$$EE^* = A_0^2 \approx F_1(z) - \eta^2 F_{2\eta}(z) - \tau^2 F_{2\tau}(z), \tag{18}$$

where

$$F_1(z) = \frac{A_{00}^2}{f^2 g} n^{2n} \exp(-2n), \tag{19}$$

$$F_{2\eta}(z) = 2\frac{A_{00}^2}{f^2 g} n^{2n} \exp(-2n), \tag{20}$$

and

$$F_{2\tau}(z) = \frac{A_{00}^2}{f^2 g} n^{2n} \exp(-2n)\frac{1}{\tau_L^2 g^2}. \tag{21}$$

Using Eqs. (4), (16), (18), (19), (20), and (21) one may express the $\varepsilon_0(z)$, $\varepsilon_{2\eta}(z)$, and $\varepsilon_{2\tau}(z)$ as

$$\varepsilon_0(z) = 1 - \frac{\omega_p^2}{\omega^2}\left[1 + \frac{a^2}{f^2 g} n^{2n} \exp(-2n)\right]^{-1/2}, \tag{22}$$

$$\varepsilon_{2\eta}(z) = \frac{\omega_p^2}{\omega^2}\frac{2a^2}{f^2 g} n^{2n} \times \exp(-2n)\left[1 + \frac{a^2}{f^2 g} n^{2n} \exp(-2n)\right]^{-3/2}, \tag{23}$$

$$\varepsilon_{2\tau}(z) = \frac{\omega_p^2}{\omega^2}\frac{a^2}{f^2 g} n^{2n} \times \exp(-2n)\frac{1}{\tau_L^2 g^2}\left[1 + \frac{a^2}{f^2 g} n^{2n} \exp(-2n)\right]^{-3/2}, \tag{24}$$

where $a = eA_{00}/m\omega c$ is the normalized laser field amplitude.

The DHG pulse profile in plasma can be obtained by solving the following two coupled second-order ODEs for the self-focusing parameter $f(z)$ and self-compression parameter $g(z)$ [obtained by substituting Eqs. (14), (15), (16), (22), (23), and (24) in Eq. (13)]:

$$\varepsilon_0(z)\frac{d^2 f(z)}{d\xi^2} = \frac{4}{\rho_0^4 f(z)^3} - \frac{1}{\rho_0^2 f(z)}\varepsilon_{2\eta}(z), \tag{25}$$

$$\varepsilon_0(z)\frac{d^2 g(z)}{d\xi^2} = \frac{1}{(\omega/c)^4 \tau_L^4 g(z)^3} - \frac{g(z)\varepsilon_{2\tau}(z)}{(\omega/c)^2}, \tag{26}$$

where $\xi = \omega z/c$ and $\rho_0 = r_0\omega/c$. For an initial plane wave the boundary conditions on Eqs. (25) and (26) are taken at $\xi = 0$ as

$$\frac{df}{d\xi} = \frac{dg}{d\xi} = 0 \text{ and } f = g = 1.$$

Equations (25) and (26) can be numerically integrated using the initial boundary conditions above to evaluate the beam width parameter f and pulse width parameter g as a function of z. The numerical estimation of f and g as a function of propagation distance will allow us to predict the variation of pulse width and beam radius of dark hollow Gaussian pulse in relativistic plasma. For $n = 0$ (Gaussian laser pulse), we may recover [from Eqs. (22)–(26)] the same results as obtained by Sharma and Kourakis [45] for relativisitc Gaussian laser pulse propagating through homogeneous plasma.

We may conclude this analytical part where we have derived a set of coupled envelope equations for the evolution of the transverse beam size and temporal pulse length of a DHG pulse. This clearly illustrates the simultaneously operating processes of focusing and compression in a plasma. The electric field of a DHG laser pulse [as given by Eq. (1)] can be analyzed as it advances in medium. We emphasize that these equations provide a picture which is arguably somewhat

idealized, since we have assumed that one spot size describes the beam at any instant t.

III. NUMERICAL INVESTIGATION

We have performed an extensive numerical investigation of the DHG pulse dynamics for the following laser plasma parameters: $a = 0.1$, $\lambda = 800$ nm, $r_0 = 20$ μm, $\tau_0 = 1$ ps, and $\omega_p^2/\omega^2 = n_e/n_c = 0.4$. We have numerically integrated Eqs. (25) and (26) (using the initial boundary conditions stated above) to evaluate the beam width parameter f and pulse width parameter g as functions of the distance of propagation z. The numerical evaluation of f and g is used to obtain the spatiotemporal evolution of dark hollow pulse intensity profile [as given by Eq. (17)] in a plasma medium at different propagation distance ξ (equivalent to a fixed time).

In Figs. 2(a)–2(d), the normalized intensity profile of a DHG pulse is depicted at a fixed distance (equivalent to a fixed propagation time), $z = 0, 754$ μm, 794 μm, and 1540 μm. The plots in Fig. 2 show the transverse focusing of the laser pulse, which is followed by longitudinal pulse compression due to the relativistic mass variation in plasma. The numerical results suggest that transverse focusing competes with the process of longitudinal self compression. The interplay between the longitudinal self compression and transverse self focusing also resulted into the merging of two intensity maxima of DHG pulse [as in shown in Figs. 2(a)–2(d)]. The merging of two maxima of DHG pulse corresponds to the convergence of intenisty maxima towards $R = 0$. We further explain the merging of two maxima in following plots as shown in Figs. 2(i)–2(l). In this way, we also observe the varying dipole potentials of a hollow beam as it propagates in the plasma. The numerical results obtained here show the spatial focusing and temporal compression of relativistic DHG pulses in homogenous plasma and confirm that the propagation behavior of Gaussian laser pulses is similar in homogeneous and inhomogeneous plasma [45] and in electron-positron plasma [46].

Figures 2(e)–2(h) show the evolution of normalized intensity as a function of time (near the radial axis, i.e., $R = 0.1$) along the direction of propagation at the same propagation distance as in Figs. 2(a)–2(d).The temporal evolution of the DHG pulse has been obtained using the same laser-plasma parameters as in Fig. 2. Our numerical results suggest an appreciable compression of the DHG laser pulse as it advances through the plasma. The temporal compression of the DHG pulse has its origin in the relativistic variation of the moving electron mass during laser-plasma interaction. We also show the evolution of normalized intensity as a function of the radial distance (around the temporal axis, i.e., $T = 0$) as shown in Figs. 2(i)–2(l). These plots give a more clear picture to observe the convergence of two intensity maxima towards the origin along the radial axis.

In Fig. 3 we have shown the normalized intensity profile of the DHG pulse, initially (at $z = 0$) and at a fixed propagation distance (equivalent to a fixed time), as the beam propagates in the plasma for various higher orders of DHG pulse. The results are depicted in Fig. 3. At propagation distance $z = 0$

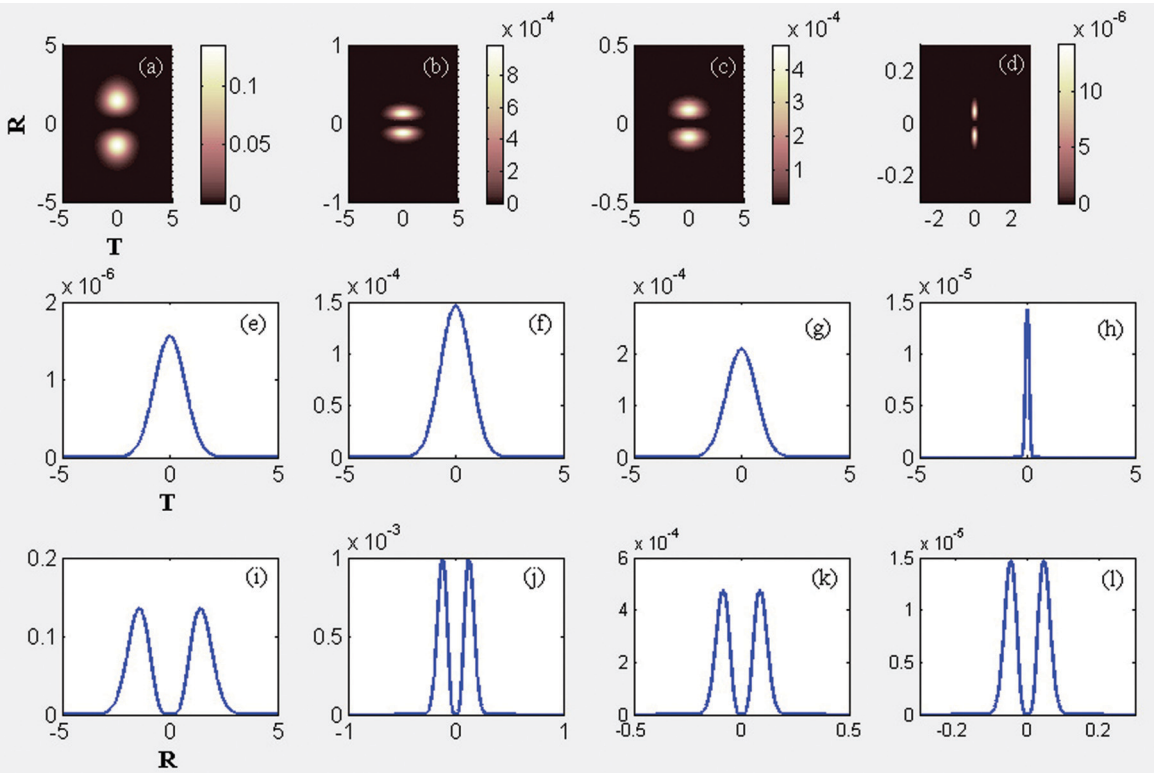

FIG. 2. (Color online) The normalized intesity of the DHG laser pulse ($n = 1$) is depicted at a fixed distance (equivalent to a fixed propagation time) in the plasma. The x and y axes, respectively, present the $T = \tau/\tau_L$ in time coordinate and $R = r/r_0$ in space coordinate. The color bar shows the variation in the normalized intensity.

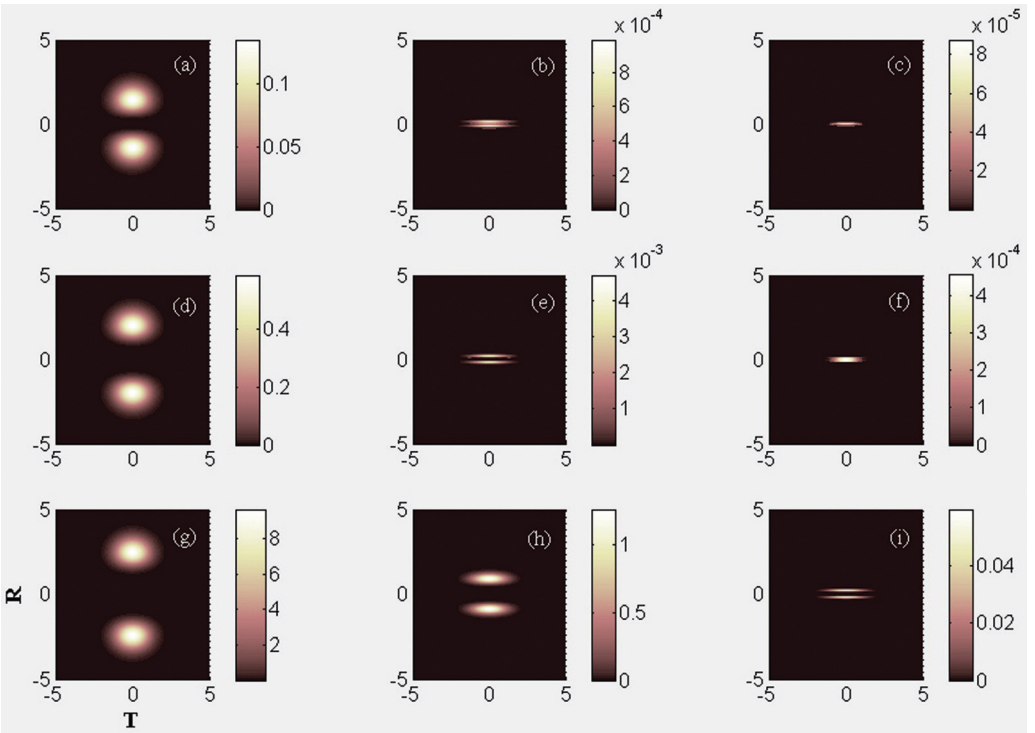

FIG. 3. (Color online) DHG pulse evolution: the variation of the normalized intensity with radial distance r and time t is shown at different propagation distance (equivalent to fixed time). The results are shown for different n values: $n = 1$ (top row), 2 (second row), 3 (third row). The x and y axes, respectively, present the $T = \tau/\tau_L$ in time coordinate and $R = r/r_0$ in space coordinate. The color bar shows the variation in the normalized intensity.

[Figs. 3(a), 3(d), and 3(g)], $z = 794$ μm [Figs. 3(b),3(e), and 3(h)], and $z = 1200$ μm [Figs. 3(c),3(f), and 3(i)]. We note that the dark region increases if one considers a higher-order DHG pulse. The numerical results confirm the convergence of the two maxima of the DHG pulse as it advances in nonlinear plasma. The initial laser-plasma parameters are considered the

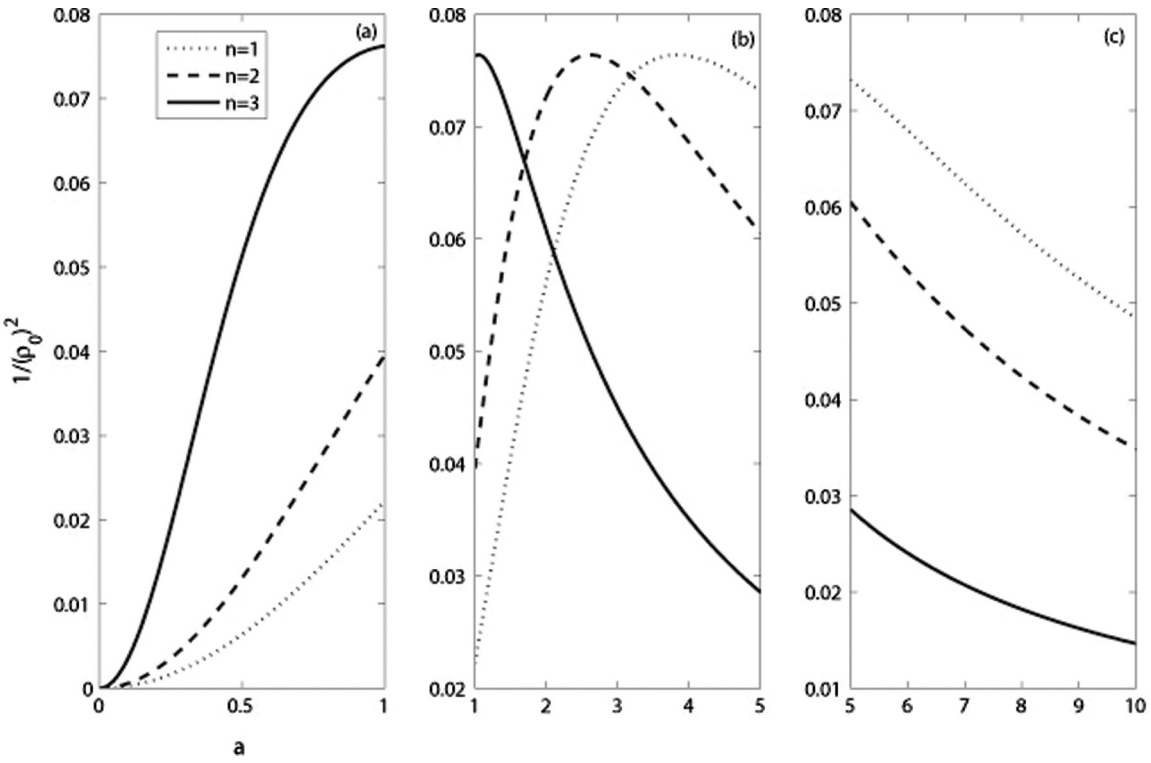

FIG. 4. Critical curves of DHG laser pulses.

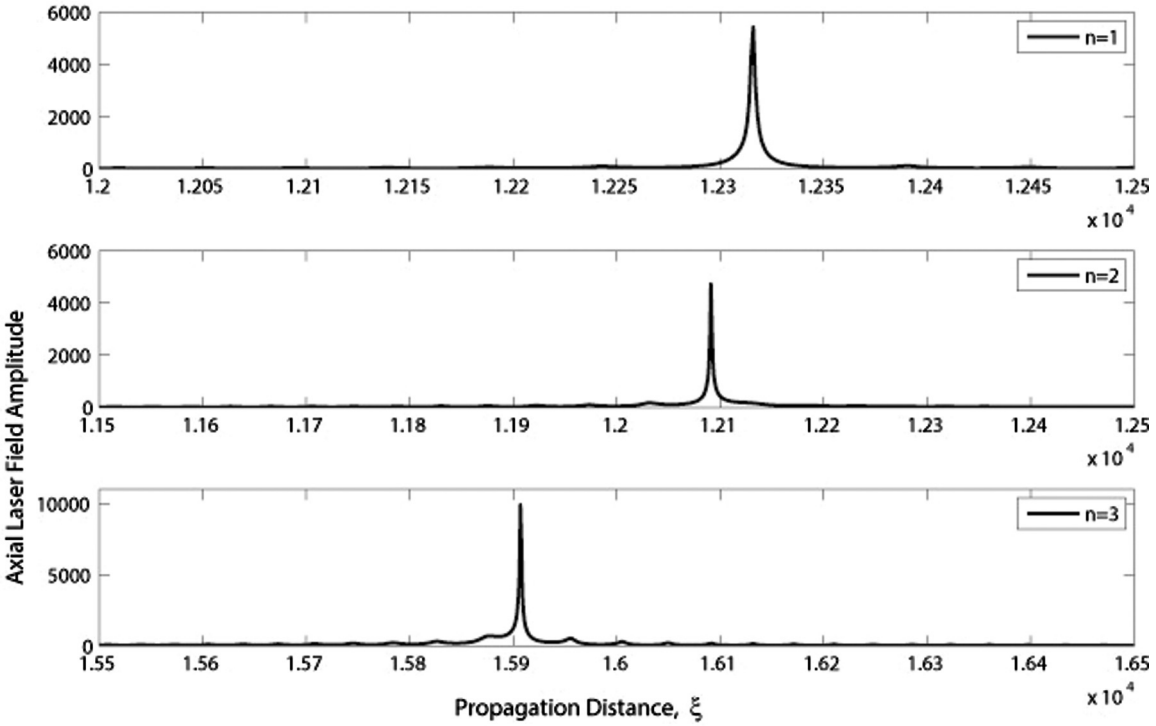

FIG. 5. The axial laser field of DHG laser pulse at a fixed propagation distance for $n = 1$, 2, and 3.

same as in Fig. 2 for all three modes $n = 1$, 2, and 3. The complex amplitude of the laser field [as given by Eq. (14)] depends on the order of the DHG pulse. Therefore, while considering the same initial laser-plasma parameters, a higher-order DHG pulse shows high intensity, although it falls in the same nonlinear regime as $n = 1$. To make it more clear, we depict the critical condition in terms of the beam size and the laser field strength in Fig. 4. Figure 4 shows the critical condition for beam convergence or divergence, corresponding to a set of given initial values of laser-plasma parameters. We show here that in the $n = 3$ case, lower divergence occurs, in comparison to $n = 1$ and 2. In this way, if we choose the same initial laser-plasma parameters, a different nonlinear regime may occur, as can be seen in Fig. 4.

Figure 4 shows the critical curves for DHG pulses ($n = 1$, 2, and 3). The curves depicted show the relation between the initial normalized field (a) and the initial dimensionless beam width (ρ_0). The critical curves can be obtained using the initial boundary conditions ($\xi = 0$, $f = g = 1$, $\frac{d^2 f(z)}{d\xi^2} = 0$) in transverse pulse propagation [Eq. (25)], as given below:

$$\frac{1}{\rho_0^2} = \frac{\omega_p^2}{\omega^2}\frac{a^2 n^{2n}\exp(-2n)}{2}\left[1 + a^2 n^{2n}\exp(-2n)\right]^{-3/2}. \quad (27)$$

The region below the curves in the ($\frac{1}{\rho_0^2}$-a) space [corresponding to $n = 1$ (dotted curve), $n = 2$ (dashed curve), and $n = 3$ (solid curve)] defines the region of convergence while the region above these curves corresponds to the divergence region. The curves are of high relevance to explore the focusing and defocusing conditions of DHG laser pulse for given initial laser-plasma parameters. From Fig. 4(a), we see clearly that a high-order DHG pulse ($n = 3$) presents limited divergence, compared to $n = 2$ case, which in turn represents lower divergence than $n = 1$ case. The critical curves [as shown in Fig. 4(a)] correspond to typical laser plasma parameters for which our model is valid in the relativistic regime. However, for illustration and comparison purposes, we provide also the critical curves obtained in the strongly relativistic case [as shown in Figs. 4(b) and 4(c)], which is admittedly not covered by our model. Figures 4(b) and 4(c) show that the less divergent nature of higher-order DHG pulses is not valid for strong laser fields.

Using Eq. (14) for the laser field amplitude, one may find the dependence of the electric field amplitude $E(\eta,\tau,\xi)$ on n around the axis $\eta = 0$ and $\tau = 0$, as $A_0(\eta = 0,\tau = 0,\xi) = A_{00} n^n \exp(-n)/f(z)g(z)^{1/2}$. This analytical formulation reflects the dependence of the axial laser field amplitude on the order of the DHG laser pulse. In order to trace the dependence of the normalized axial amplitude on the order of DHG pulse n, we have numerically evaluated the axial laser field amplitude at focusing length along the propagation distance ξ (for different values of the n); the results are shown in Fig. 4. The laser-plasma parameters considered are the same as in Figs. 2–4. Figure 5 shows that the intensity peaks are higher for higher n and that these peaks represent the foci (beam intensity maxima) corresponding to higher n values.

IV. CONCLUSIONS

Dark hollow beams have interesting physical properties and are of relevance in various physical contexts. Interestingly, such beams may exhibit a nondiffracting behavior on propagation. Most of the known theoretical models to describe dark hollow beams consider a transverse intensity distribution.

In contrast to earlier studies based on a transverse intensity distribution of DHG pulses, our analysis takes into account a realistic physical picture and incorporates both the transverse and temporal intensity distribution(s).

We have investigated the spatiotemporal dynamics of dark hollow Gaussian relativistic laser pulses in a plasma. We have developed an analytical model (relying on the approach introduced earlier by Sharma and Kourakis [44] and Sodha *et al.* [34]) for pulse propagation in a plasma. In summary, we have modeled the complex spatiotemporal evolution of the electric field of a DHG laser pulse in a plasma, which may [using Eqs. (1) and (8)] be expressed as

$$E(r,z,t) = A_0(r,z,\tau)\exp[-ikS(r,z,\tau)](e_x + ie_y) \times \exp[i(kz-\omega t)], \quad (28)$$

where $A_0(r,z,\tau)$ and $S(r,z,\tau)$ are given by Eqs. (14) and (15). The evolution of a DHG laser field in plasma can be evaluated using the coupled second-order differential equations (25) and (26). A set of numerical simulations have enabled us to trace the spatial and temporal evolution of a higher-order DHG pulse. We have observed the merging of (the peaks of) a DHG pulse due to nonlinear relativistic effects, as the pulse propagates in the plasma, that is, the convergence of the beam's two intensity maxima along the radial axis towards the origin.

In conclusion, we have identified both focusing and compression mechanisms operating during propagation of a dark hollow pulse ($n = 1, 2$, and 3) in a plasma medium. Such focused and compressed dark hollow Gaussian laser pulses can be generated in experiments, which will be relevant in particle trapping. The typical laser-plasma parameters for experiment purposes can be predicted by using this model, with an aim to control the focusing and compression processes of DHG pulses in plasma. In practical terms, one may tune DHG pulses while using a weakly relativistic normalized laser field ($a < 1$) with pulse length much greater than the plasma wavelength, with plasma density ranging from quarter-critical to the critical value. Our theoretical and numerical results confirm (as predicted earlier [37]) that higher-order DHG pulses suffer smaller divergence as they propagate and, thus, lead to enhanced energy transport in the weakly relativistic field regime.

ACKNOWLEDGMENTS

I.K. acknowledges financial support from the UK Engineering and Physical Sciences Research Council (EPSRC) under Grant No. EP/I031766/1.

[1] A. Goban, K. S. Choi, D. J. Alton, D. Ding, C. Lacroute, M. Pototschnig, T. Thiele, N. P. Stern, and H. J. Kimble, Phys. Rev. Lett. **109**, 033603 (2012).
[2] A. Ashkin, Phys. Rev. Lett. **40**, 729 (1978).
[3] M. J. Renn, D. Montgomery, O. Vdovin, D. Z. Anderson, C. E. Wieman, and E. A. Cornell, Phys. Rev. Lett. **75**, 3253 (1995).
[4] P. Londero, V. Venkataraman, A. R. Bhagwat, A. D. Slepkov, and A. L. Gaeta, Phys. Rev. Lett. **103**, 043602 (2009).
[5] M. Bajcsy, S. Hofferberth, V. Balic, T. Peyronel, M. Hafezi, A. S. Zibrov, V. Vuletic, and M. D. Lukin, Phys. Rev. Lett. **102**, 203902 (2009).
[6] E. Vetsch, D. Reitz, G. Sague, R. Schmidt, S. T. Dawkins, and A. Rauschenbeutel, Phys. Rev. Lett. **104**, 203603 (2010).
[7] S. T. Dawkins, R. Mitsch, D. Reitz, E. Vetsch, and A. Rauschenbeutel, Phys. Rev. Lett. **107**, 243601 (2011)
[8] Y. Cai, X. Liu, and Q. Lin, Opt. Lett. **28**, 1084 (2003).
[9] Yu. B. Ovchinnikov, I. Manek, and R. Grimm, Phys. Rev. Lett. **79**, 2225 (1997).
[10] Y. Song, D. Milam, and W. T. Hill, Opt. Lett. **24**, 1805 (1999).
[11] J. Yin, Y. Zhu, W. Jhe, and Y. Wang, Phys. Rev. A **58**, 509 (1998).
[12] T. Kuga, Y. Torii, N. Shiokawa, T. Hirano, Y. Shimizu, and H. Sasada, Phys. Rev. Lett. **78**, 4713 (1997).
[13] X. Xu, Y. Wang, and W. Jhe, J. Opt. Soc. Am. B **17**, 1039 (2000).
[14] J. Yin, W. Gao, H. Wang, Q. Long, and Y. Wang, Chin. Phys. **11**, 1157 (2002).
[15] I. Gerdova, X. Zhang, and A. Hache, *Lasers and Electro-Optics, Quantum Electronics and Laser Science Conference* (IEEE, CA, 2006), pp. 1–2.
[16] S. Konar and S. Jana, Phys. Scr. **71**, 198 (2005).
[17] J. Arlt and K. Dholakia, Opt. Commun. **177**, 297 (2000).
[18] M. A. Clifford, J. Arlt, J. Courtial, and K. Dholakia, Opt. Commun. **156**, 300 (1998).
[19] J. Arlt, T. Hitomi, and K. Dholakia, Appl. Phys. B **71**, 549 (2000).
[20] M. Zhang and D. Zhao, J. Opt. Soc. Am. A **22**, 1898 (2005).
[21] Y. Cai and L. Zhang, J. Opt. Soc. Am. B **23**, 1398 (2006).
[22] J. Turunen, A. Vasara, and A. T. Friberg, Appl. Opt. **27**, 3959 (1988).
[23] X. Wang and M. G. Littman, Opt. Lett. **18**, 767 (1993).
[24] L. Zhang, X. Lu, X. Chen, and S. He, Chin. Phys. Lett. **21**, 298 (2004).
[25] J. Yin, H. Noh, K. Lee, K. Kim, Yu Wang, and W. Jhe, Opt. Comm. **138**, 287 (1997).
[26] N. R. Heckenberg, R. Mcduff, C. P. Smith, and A. G. White, Opt. Lett. **17**, 221 (1992).
[27] A. Vasara, J. Turunen, and A. T. Friberg, J. Opt. Soc. Am. A **6**, 1748 (1989).
[28] D. Ganic, X. Gan, M. Gu, M. Hain, S. Somalingam, S. Stankovic, and T. Tschudi, Opt. Lett. **27**, 1351 (2002).
[29] Y. Cai and S. He, J. Opt. Soc. Am. A **23**, 1410 (2006).
[30] Y. Cai and L. Zhang, Opt. Express **14**, 1353 (2006).
[31] Z. Gao and B. Lu, Chin. Phys. Lett. **23**, 106 (2006).
[32] Z. Mei and D. Zhao, J. Opt. Soc. Am. A **23**, 919 (2006).
[33] G. Zhou, J. Opt. **13**, 075711 (2011).
[34] M. S. Sodha, S. K. Mishra, and S. Misra, Laser Part. Beams **27**, 57 (2009).
[35] M. S. Sodha, S. K. Mishra, and S. Misra, J. Plasma Phys. **75**, 731 (2009).
[36] S. Misra and S. K. Mishra, Prog. Electromagn. Res. B **16**, 291 (2009).
[37] A. Sharma, M. S. Sodha, S. Misra, and S. K. Mishra, Laser and Particle Beams, doi: 10.1017/S0263034613000402 (in press).
[38] Y. Xu and B. Lu, J. Opt. A: Pure Appl. Opt. **9**, 496 (2007).

[39] R. W. Boyd, S. G. Lukishova and Y. R. Shen, *Self-focusing: Past and Present* (Springer-Verlag, New York, 2009), 114.
[40] O. Shorokhov, A. Pukhov, and I. Kostyukov, Phys. Rev. Lett. **91**, 265002 (2003).
[41] F. S. Tsung, C. Ren, L. O. Silva, W. B. Mori, and T. Katsouleas, Proc. Natl. Acad. Sci. USA **99**, 29 (2002).
[42] C. Ren, B. J. Duda, R. G. Hemker, W. B. Mori, T. Katsouleas, T. M. Antonsen, Jr., and P. Mora, Phys. Rev. E **63**, 026411 (2001).
[43] S. Shibu, J. Parashar, and H. D. Pandey, J. Plasma Phys. **59**, 91 (1998).
[44] A. Sharma, J. Borhanian, and I. Kourakis, J. Phys. A: Math. Theor. **42**, 465501 (2009).
[45] A. Sharma and I. Kourakis, Plasma Phys. Contr. Fusion **52**, 065002 (2010).
[46] A. Sharma, I. Kourakis, and P. K. Shukla, Phys. Rev. E **82**, 016402 (2010).
[47] T. M. Antonsen and P. Mora, Phys. Rev. Lett. **69**, 2204 (1992).
[48] P. Sprangle, E. Esarey, and A. Ting, Phys. Rev. Lett. **64**, 2011 (1990).
[49] M. D. Feit, J. C. Garrison, and A. M. Rubenchik, Phys. Rev. E **53**, 1068 (1996).